Dynamic interplay between a TonB dependent heme transporter and a TonB protein in a membrane environment

Kamolrat Somboon[1], Oliver Melling[1], Maylis Lejeune[2], Glaucia M.S. Pinheiro[2], Annick Paquelin[3], Benjamin Bardiaux[2], Michael Nilges[2], Philippe Delepelaire[3], Syma Khalid[1,4*], Nadia Izadi-Pruneyre[2*]

[1]School of Chemistry, University of Southampton, Southampton S017 1BJ, United Kingdom. [2]Institut Pasteur, Université Paris Cité, CNRS UMR3528, Structural Bioinformatics Unit, F-75015 Paris, France. [3]Institut de Biologie Physico-Chimique, UMR 7099, CNRS Université de Paris, 13 rue Pierre et Marie Curie, Paris, France. [4]Department of Biochemistry, University of Oxford, Oxford, OX1 3QU, United Kingdom.

*Corresponding authors: Syma Khalid & Nadia Izadi-Pruneyre

Email: syma.khalid@bioch.ox.ac.uk, nadia.izadi@pasteur.fr

Abstract

The envelope of Gram-negative bacteria is composed of a double membrane separated by the periplasmic space. This organization imposes geometrical and distance constraints that are key for the mechanism of action of multicomponent systems spanning the envelope. However, consideration of all three compartments by experimental approaches is still elusive. Here we used the state-of-the-art molecular dynamics simulation in an *Escherichia coli* envelope model to obtain a dynamic view of molecular interactions between the outer membrane heme transporter HasR and the inner membrane TonB-like protein HasB. Their interaction allows the transfer of the inner membrane proton motive force derived energy to the transporter for heme internalization. The simulations which incorporate both membranes show the key role of periplasmic domains of both proteins, and their dynamics in the complex formation and stability. They revealed a previously unidentified atomic network of interactions, as well as the sequences of the interactions and their variations with the presence of external substrates. Experimental validation (mutations, phenotypic and *in vitro* assays) confirms the robustness of our approach and provides verification of the simulation-predicted interactions. Based on structural and sequence conservation, the network of interaction revealed in this study is expected to occur in other nutrient import systems. The integrative approach presented here is highly useful to study the dynamic interplay between components of any other bacterial transmembrane systems.

Introduction

Gram-negative bacteria are delimited by an envelope composed of two membranes (outer membrane, OM and inner membrane, IM) separated by the periplasmic space. The IM TonB complex and the specific OM TonB-dependent transporters (TBDTs) are used to import scarce and essential nutrients, such as metal sources, vitamin B_{12}, some specific carbohydrates, etc (1, 2). As both the OM and the periplasm lack an energy source, the TonB complex is used to couple substrate entry to the proton-motive force provided by the proton gradient across the IM.

The TonB complex comprises three IM proteins, TonB, ExbB and ExbD. TonB is the only protein of the complex interacting directly with the TBDT and thus transferring the energy, whereas ExbB and ExbD, forming a proton-channel, are considered as the engine of the system (3). The structure of the complete TonB complex and of the full-length TonB protein are still unknown. TonB is composed of a N-terminus transmembrane helix inserted into the IM, an unstructured proline-rich domain in the periplasm followed by a C-terminal and globular domain that is the only identified domain of interaction with TBDT. Only the structure of this globular periplasmic domain of TonB, either alone or in complex with TBDT, have been reported (4–8). TonB interacts with the TonB-box, a stretch of 7-10 conserved residues, exposed in the periplasm and located at the N-terminus of TBDT. It is assumed that upon this interaction and in the presence of energy, by either a rotation (comparable to the Mot flagellar system)(9) or a linear movement of TonB, some conformational changes of the TBDT occur, eventually opening a channel for the entry of the substrate. This energising mechanism is not well understood yet due to the lack of structural and interaction data on the whole system.

Here we use the heme acquisition system (Has) to get insight into the dynamic interplay between a TBDT and a TonB protein. The Has is developed by commensal and pathogenic bacteria to acquire heme that is their major iron source in mammals. The system studied here is from *Serratia marcescens* and reconstituted in *Escherichia coli*. It is composed of the TBDT HasR functioning in synergy with a hemophore (HasA) that harvests extracellular heme, either free or bound to host hemoproteins (like hemoglobin). Heme is then transferred from HasA to HasR to be internalized, the complex formed by HasA-HasR is dissociated, and HasA is recycled into the external medium. The two steps of heme internalization and recycling of HasA need energy that is provided by HasB, a TonB paralog dedicated to the Has system(10–12) .

HasR has the same structural organization as other TBDTs, with a 22-stranded β-barrel forming a trans-membrane domain anchored in the OM, with 11 extracellular loops and 11 periplasmic loops. The region upstream this domain folds inside the barrel, forming the so-called “plug”(1). HasR belongs to a class of TBDTs coupled to a signalling activity. In these TBDTs, the TonB-box is not at the extreme N-terminus, but is connected to a periplasmic globular domain called the signalling

68 domain, or $HasR_{SD}$ in HasR(13). $HasR_{SD}$ sends the signal of the presence of extracellular sources
69 of heme (heme and HasA) to an anti-sigma/ECFσ factor pair which activates the expression of the
70 *has* operon (10).
71 Previously we combined the X-ray structure of HasR (14), the NMR structure of $HasR_{SD}$ with
72 electron microscopy (EM) density maps and SAXS data, to obtain a structural model of the full-
73 length HasR in its free form and in complex with HasA and heme (holo-HasR). This model showed
74 for the first time the structure of a full-length TBDT, with the signalling domain projected far from
75 the β-barrel (at 8 and 7 nm in the apo- and holo-form, respectively)(13) *via* a flexible linker. A similar
76 location of the signalling domain with respect to the β-barrel was recently shown in the X-ray
77 structure of FoxA from *Pseudomonas aeruginosa*(8).
78 HasR and HasB interact through their periplasmic exposed regions. In previous work, we solved
79 the structure of the C-terminal and periplasmic domains of HasB ($HasB_{CTD}$)(15) and studied its
80 interaction with a peptide containing the TonB-box of HasR ($G_{95}ALALDSL_{102}$). We showed that an
81 ionic interaction between HasR (D_{100}) and HasB (R_{169}) is crucial for the stability of this interaction
82 and for HasR function. Furthermore, by using isothermal titration microcalorimetry (ITC), we
83 showed that heme and HasA modulate the thermodynamic parameters and the network of
84 interactions(16). However, the precise nature of the interactions, their variations and the interacting
85 residues remained unknown.
86 HasR and HasB are inserted into two different membranes that are separated by the periplasmic
87 space. To characterise the HasR-HasB interaction, it is therefore critical to consider the spatial
88 constraints imposed by the membranes, in particular the distance between them together with the
89 protein dynamics. In this work, to develop a more thorough view of the HasR-HasB interaction, we
90 have combined our structural and interaction data to model the protein complex in the context of *in*
91 *silico* models of the IM and OM. We performed molecular dynamics (MD) simulations of the
92 HasR+HasB system in apo- and holo-forms, that is to say in the presence of heme and HasA
93 (holoHasR+HasB). The simulations revealed a previously unidentified network of interactions and
94 the key role of particular periplasmic loops in the complex formation and stability. We
95 experimentally validated the network of interactions by mutations, and phenotypic and *in vitro*
96 assays. Interestingly, the interactions are modulated by the external signal consisting in the
97 presence of heme and HasA. This work represents the first example showing the molecular details
98 of the interaction of a TBDT with a TonB like protein with inclusion of both membranes. The

sequence of events and the movements observed during the simulations provide a more detailed understanding of the mechanism of energy and signal transfer through the bacterial cell envelope.

Results

Molecular Dynamics of the HasR-HasB complex

We started by the simplest system (HasR-HasB) consisting of HasR in apo-form (without its extracellular substrates) and HasB (Figure 1). We constructed an initial model of these two proteins each in a membrane model based on their structural organization, and guided by our previous experimental findings, as described in the supplementary Information. In the HasR model, the linker was almost fully extended at a distance of 11.5 nm from the barrel. The $HasB_{CTD}$ is located at ~ 6.8 nm from the HasR barrel (centre of mass measurements). The HasB transmembrane domain is a single helix located in the model IM. The two membranes are separated by ~ 12 nm, this is the shortest distance (the distance from the centre of the OM to the centre of the IM is ~ 16 nm). This was deemed to be a good compromise between the average of the periplasmic thicknesses reported in the literature and keeping the simulation system size practical. (Figure 1)

Visual observations

On performing two initial simulations of the HasR-HasB model as described above, in one of the simulations we noted interaction of two periplasmic loops of HasR with $HasB_{CTD}$ (discussed in detail later), so we initiated two additional simulations of the HasR-HasB complex from a point at which the contact between the loops of HasR and HasB has already been established (Figure 1). Thus, overall we simulated the HasR-HasB complex as (1) HasR-HasB in which wild-types of both proteins are considered in the original model (2 x 300 ns), (2) int-HasR-HasB in which the simulations are initiated after the contact with the loops has been made (4 x 300 ns), and (3) HasR-HasB with a periplasmic space at 23 nm called the wide periplasm hereafter (4 x 50 ns) (4) $HasR_{mutants}$-HasB in which different periplasmic loops of HasR are mutated as described below (2 x 300 ns per mutant).

Secondary structure and structural integrity

Given that the starting conformations of the complexes we are simulating are models, albeit based on structural data and guided by experimental data, we first evaluated the structural integrity of the folded domains. The root mean square deviation (RMSD) from the initial model and the secondary structures were evaluated. In all cases, we observed that the protein structural deviation is within acceptable ranges based on simulations of similar proteins and there is no significant unfolding of the structured domains. The RMSD, root mean square fluctuation (RMSF) and secondary structure

analysis of one simulation of each system are provided in the supplementary information (Figure S1).

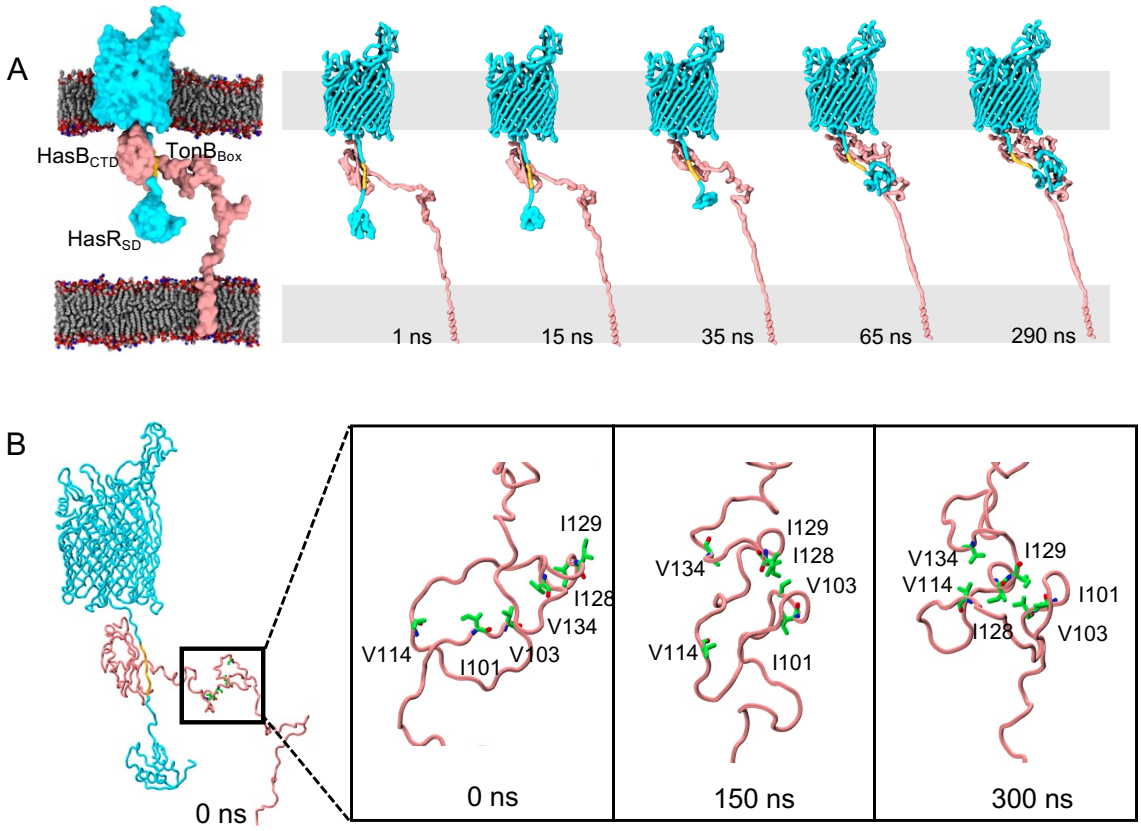

Figure 1. The HasR-HasB complex. A. PCA analysis. *HasR is cyan and HasB is pink. Left: Initial model of the HasR-HasB complex at time = 0 ns. Each protein is embedded in a model membrane. The membrane lipids are grey, red and blue, the TonB box is in yellow, water and ions are omitted for clarity. Proteins are shown in surface representation, while membrane is shown as spheres. Right: Spontaneous interaction between HasB and HasR periplasmic loops. Here only the protein backbones are included in the surface representation. Projection along the first principle component from the HasR-HasB simulation at 1, 15, 35, 65 and 290 ns.* ***B. Hydrophobic contacts along the HasB proline-rich domain****. The panel on the left shows the location of the hydrophobic residues at 0 ns. The close-up version on the right shows this domain becoming less extended during the simulation. Key hydrophobic residues in HasB are shown as sticks and labelled.*

Inter-protein motion

The long disordered periplasmic regions of HasR and HasB impart considerable flexibility to the complex in the periplasm. Therefore, we next explored the inter-domain and inter-protein movements. A useful way of filtering the large-scale motions is principal components analysis (PCA). We employed this method to characterise the motion along the first eigenvector for the HasR-HasB complexes in the HasR-HasB and int-HasR-HasB systems (Figure 1). Interpolation

between the extreme conformations sampled in each case shows a distinct pattern in the inter-protein motions. The principle motion in the original HasR-HasB simulations is a reduction in the distance between the $HasR_{SD}$ and the barrel, and a concomitant reduction in the distance between $HasB_{CTD}$ and $HasR_{SD}$ as shown in Figure 1 and 2.

In simulations of the int-HasR-HasB system, the major motion is a rearrangement of $HasB_{CTD}$ with respect to the HasR linker and $HasR_{SD}$ (since the large motion of $HasR_{SD}$ and $HasB_{CTD}$ had already occurred). These data strongly suggest that the HasR periplasmic region (the linker including the TonB box) is considerably flexible and that the starting model required some inter-protein adjustments in particular with respect to interactions of the $HasR_{SD}$ with $HasB_{CTD}$, given the adjustment occurred spontaneously during the simulations.

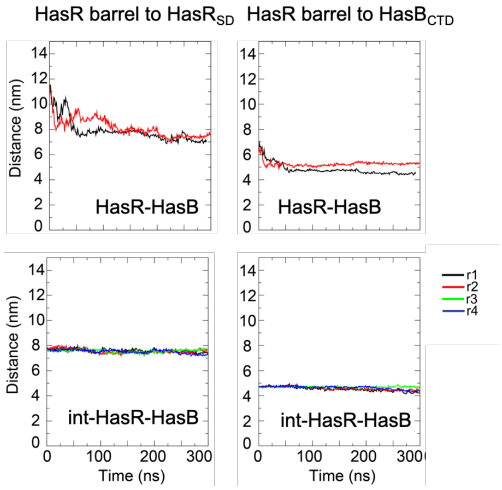

Figure 2. Intra- and inter-protein domain distances. *The panel on the left shows the minimum distance between the HasR barrel and the $HasR_{SD}$ as a function of simulation time. The panel on the right shows the minimum distance between the HasR barrel and the $HasB_{CTD}$. In each case the center of mass of the protein domain is used for the measurements. Different simulations from r1 to r4 are presented.*

In order to explore these movements in a more quantitative manner, we measured the HasR barrel-$HasR_{SD}$ and the HasR barrel-$HasB_{CTD}$ distances. In the HasR-HasB simulations there is a reduction in the HasR barrel-$HasR_{SD}$ distance from ~ 11 nm in the original model to ~7-7.5 nm by the end of both simulations, consistent with 8 nm determined in our previous work by SAXS and EM (13). Similarly, the HasR barrel to $HasB_{CTD}$ distance is decreased from ~ 6.8 nm to ~ 4.5 nm in one simulation and to ~ 5.4 nm in the other simulation. In simulations of the int-HasR-HasB system, the distances remain at ~ 7.7 and 4.7 nm respectively across all four simulations. A striking feature of these measurements is the consistency in the int-HasR-HasB simulations. Measurements for all

198 four independent simulations of each system stabilise to essentially the same value. This indicates
199 that in terms of large-scale movement, the protein domains have reached a metastable state for
200 these complexes (Figure 2).
201
202 **HasB-HasR TonB-box salt bridge**
203 In three of the four int-HasR-HasB simulations we observed a spontaneous formation of the salt
204 bridge between D_{100} of HasR TonB-box and R_{169} of HasB, which was previously identified by our
205 experimental work (15) (Figure 3). Interestingly in some simulations the interaction is disrupted
206 (defined as the minimum distance between the residues > 0.35 nm), but then reforms either for an
207 extended period or for transitory periods.
208
209 **HasR-HasB inter-protein β-sheet**
210 In the initial model the residues nearby D_{100} in HasR (93-111) are located at around 3Å from the
211 third β-strand of HasB (246-258), a distance compatible with hydrogen bonding and formation of a
212 β-sheet, in accordance with an interprotein β-sheet as observed in our previous model between
213 $HasB_{CTD}$ and a peptide containing HasR TonB-box(15). We monitored the number of backbone
214 hydrogen bonds between the two proteins in this region in each simulation (Figure 3C). There are
215 up to 5 hydrogen bonds present between residues 93-111 of HasR and residues 246-258 of
216 $HasB_{CTD}$ in any one frame of HasR-HasB and int-HasR-HasB simulations. In the HasR-HasB
217 simulations there is a reduction in the number of hydrogen bonds as the simulations proceed, such
218 that by ~ 200 ns there are generally either none or just a single hydrogen bond present in this
219 region. In the int-HasR-HasB simulations there are 2-8 hydrogen bonds throughout the simulations.
220 The number of hydrogen bonds does decrease as some of the simulations proceed. Hydrogen
221 bonding between backbone atoms is in some cases replaced by hydrogen bonds between side
222 chains in this region. Examples include the backbone hydrogen bonding interaction between HasB
223 P_{253} and HasR V_{104}, which is replaced by HasB P_{253} (backbone) to HasR T_{103} (side chain) in one of
224 the int-HasR-HasB simulations. Full details are provided in the supplementary information (Figure
225 S3). Thus, this region of interaction is labile and while the strands remain in close proximity to each
226 other, the number of hydrogen bonds fluctuates. Overall, the inter-protein contacts are more stable
227 in the int-HasR-HasB simulations, in other words once contact with HasR periplasmic loops has
228 been established. We note here that an equivalent inter-protein β-sheet was reported in the X-ray

structure of the complexes between *E. coli* $TonB_{CTD}$ and the TonB-box of the TBDT FhuA, BtuB and FoxA (6–8).

A

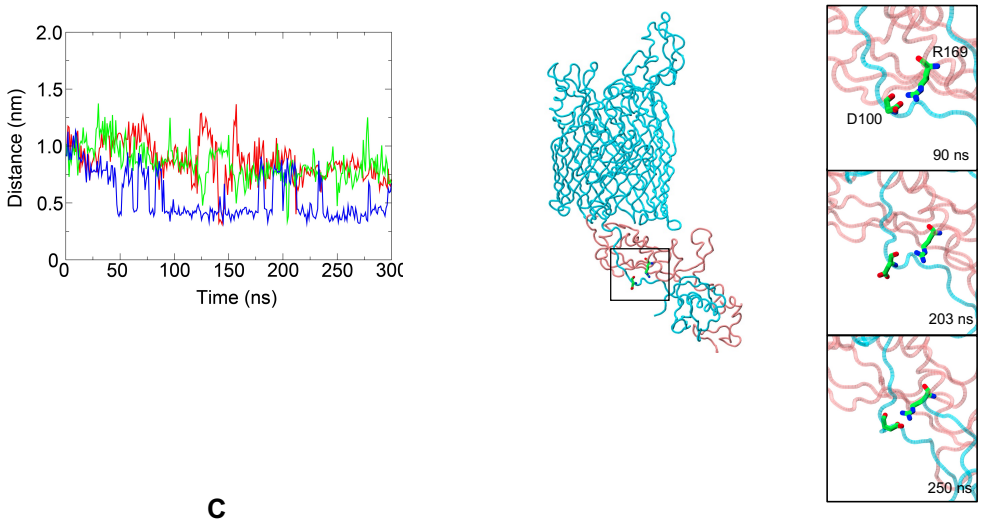

B **C**

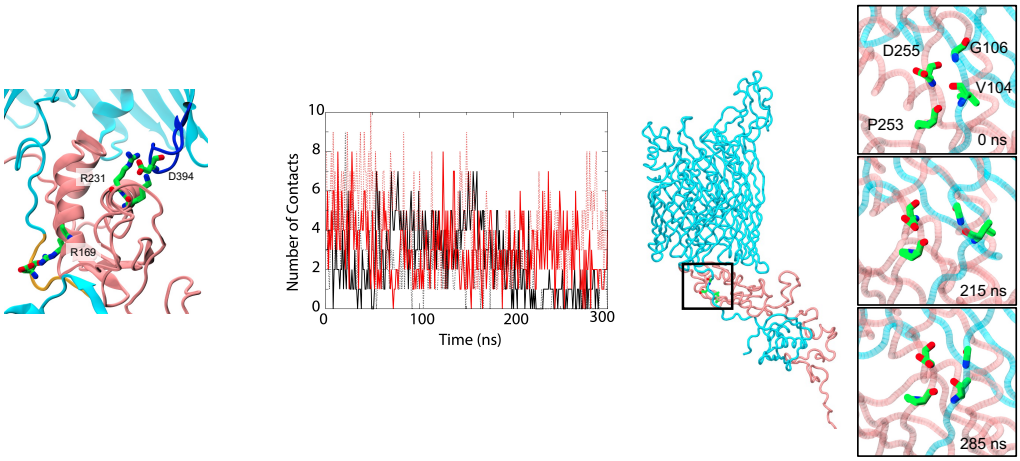

***Figure 3 HasR TonB-box and HasB interaction**. **A:** HasR TonB-box and HasB salt bridge Distance measurement between D_{100} of HasR TonB-box and R_{169} of HasB. Three simulations (in blue, red and green) are shown. **Right:** a zoomed in version of the central panel shows the two residues (D_{100} and R_{169}) from one of int-HasR-HasB simulations as an example of the reformed salt bridge during simulation. **B**: HasB-HasR TonB-box salt bridge**.** Snapshot taken from t = 250 ns of one of the int-HasR-HasB simulations, showing the HasR D_{100}-HasB R_{169} salt bridge intact. The HasR D_{394}-HasB R_{231} salt bridge is also shown. HasR, L4 and the TonB box of HasR are coloured in cyan, blue and yellow respectively. HasB residues 1 to 70 and HasR residues 430 to 600 are omitted for clarity. **C:** Hydrogen bonds within the HasR-HasB inter-protein β-sheet**.** The panel on*

the left shows the total number of hydrogen bonds between HasR residues 99-111 and HasB residues 246-258 as a function of simulation time. The panel on the right (a zoomed in version of the central panel) shows four residues (V_{104} and G_{106} of HasR and P_{253} and D_{255} of HasB) highlighted from one of the int-HasR-HasB simulations as an example of the lability in the interactions in this region. At time = 0 ns, backbone hydrogen bonding is seen between HasR V_{104} and HasB D_{255}; HasR G_{106} and HasB D_{255}, HasR V_{104} and HasB P_{253}. At 215 ns the inter-protein hydrogen bonds are broken, by 285 ns the hydrogen bond between HasR V_{104} and HasB P_{253} is reformed and the four residues are in general closer together than at 215 ns.

Interaction of HasR periplasmic loops with HasB

As already discussed, at the start of the HasR-HasB simulations there is a large inter-protein motion in which the distance between the $HasR_{SD}$ and the $HasB_{CTD}$ is reduced. In one of the simulations this movement results in interactions of HasB with HasR periplasmic loops L1 and L4, the loop numbering being from the N- to the C-terminus. The interactions formed spontaneously within about 20 ns for L1 and 50 ns for L4, and then remained stable for the duration of the simulation. The int-HasR-HasB simulations were initiated from when these loops have already made contact with $HasB_{CTD}$, and these interactions are maintained for the duration of all four simulations (4 x 300 ns). The HasR L1-HasB interactions are largely through hydrophobic contacts of A_{238} and P_{239} of HasR L1 with L_{189} of $HasB_{CTD}$ (Figure 4A, 4B).

Once the interactions with L1 are formed, the HasR linker and $HasB_{CTD}$ move with respect to each other and then $HasB_{CTD}$ contacts L4 *via* several salt bridges. The most prevalent are between either E_{393} or D_{394} of HasR L4 with either K_{230} or R_{231} of $HasB_{CTD}$ (Figure 4A, 4B). Salt bridges between E_{393} and R_{223} are also observed. While the L4-$HasB_{CTD}$ interaction exists for the duration of the 5 x 300 ns of the simulations in which it is observed, no other individual salt bridge is observed for the duration of any of these simulations. Instead, the salt bridges are observed to form, break and often reform throughout the simulations, suggesting either a protein-protein interface stabilised by non-specific interactions or that the simulations are not long enough to achieve a stabilised interface between the two proteins. Having said that, the persistence in the overall number of contacts in all five simulations between the proteins in this region does suggest that L4 is important for the interaction of HasR with the $HasB_{CTD.}$ This is further reinforced in the simulation on the $HasR_{L4}$-HasB system, $HasR_{L4}$ being a variant of HasR in which L4 (P_{392}EDVDWLD) is replaced by the sequence ATSA. The size of four residues is the minimum required to form a periplasmic loop. In these simulations the distance between the centres of mass of the $HasR_{L4}$ barrel and $HasB_{CTD}$ is ~ 5.6 nm (compared to ~ 4.5 nm in the simulations in which contact between L4 and $HasB_{CTD}$ is observed) and L4 does not come within hydrogen-bonding distance of $HasB_{CTD}$ during these

simulations (Figure 4B). Interestingly in the absence of L4-HasB interaction, the salt bridge between D_{100} of HasR TonB-box and R_{169} of HasB is not maintained.

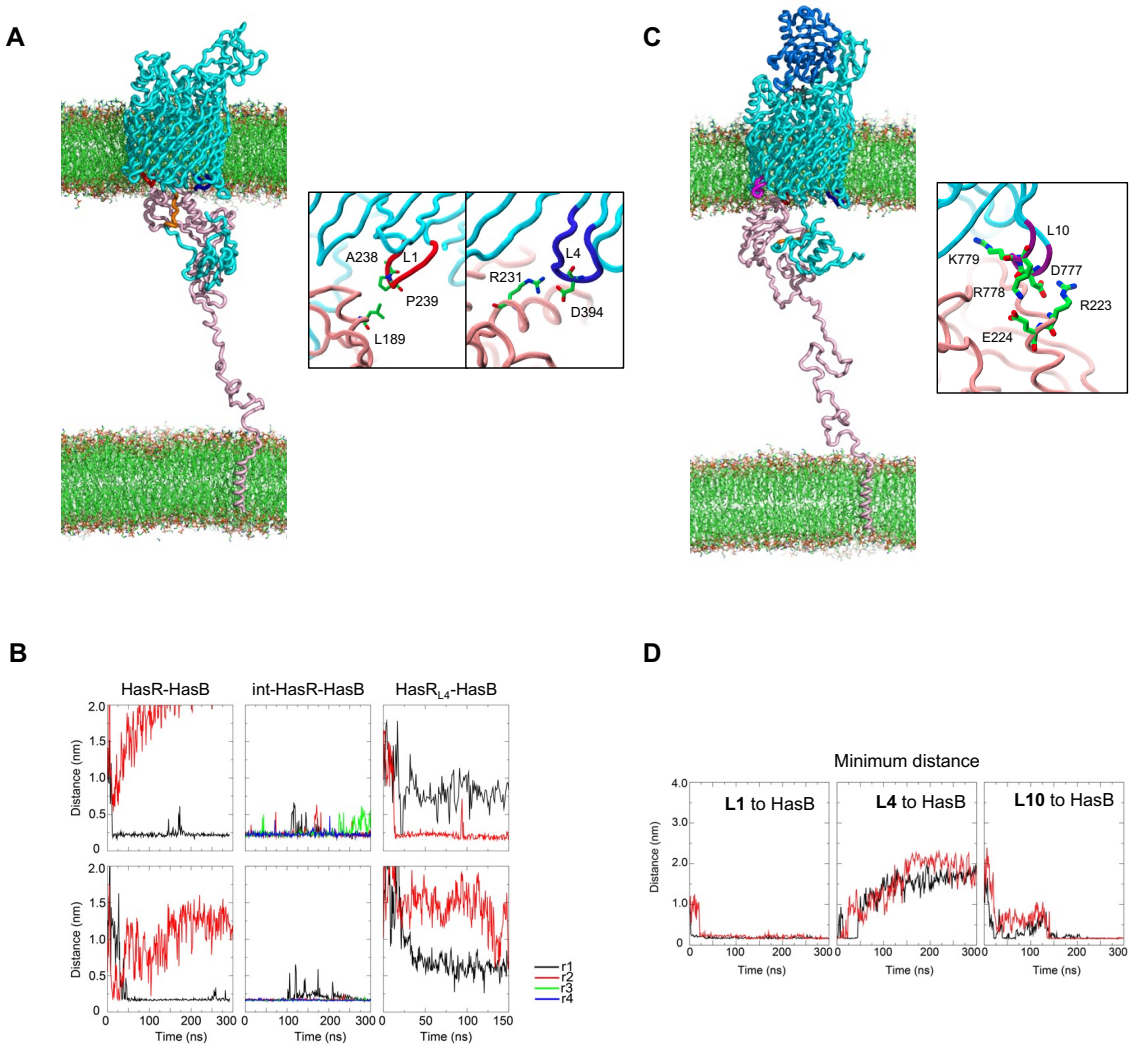

***Figure 4. Interaction of HasR periplasmic loops with HasB**. **A: HasR-HasB.** Left: Snapshot of one of the simulated HasR-HasB complex in membranes. HasR L1 and L4 are coloured in red and dark blue, respectively. The TonB box is in orange. Right: Some key residues are labelled and shown. **B**: Evolution of the minimum distance between HasR L1 (top row) or L4 (bottom row) to HasB during different HasR-HasB simulations (r1, r2, r3 and r4) are shown. The distance from the closest atoms between the loops and HasB was measured. **C: HoloHasR-HasB**. Left: Snapshot of the simulated holoHasR-HasB complex in membranes at 285 ns. Same colour codes as in A. L10 is coloured in purple. HasA in blue and heme in black**. D**: Evolution of minimum distance between HasR L1, L4 or L10 to HasB during the holoHasR-HasB simulations. Two simulations are presented, r1 in red and r2 in black.*

309 **Effect of the periplasmic thickness in the HasR-HasB interaction**

310 The HasR-HasB interaction occurs in the periplasmic space. Periplasmic thicknesses from 10 to
311 50 nm have been reported . Therefore, we investigated the effect of the periplasm thickness on the
312 HasR-HasB interactions observed in our original simulations by extending the width of the
313 periplasm to 23 nm (measuring from membrane midpoints). We constructed two models with a
314 more extended HasB proline-rich domain to span the wide periplasm and performed two
315 independent simulations of each, giving a total of 4 x 50 simulations. The hydrogen bonds between
316 residues involved in the inter-protein β-sheet (Figure S4A) and the HasRL4-HasB and HasRL1-
317 HasB (Figure S4B) interactions were maintained throughout these simulations. We also observed
318 clustering of hydrophobic residues in the HasB proline-rich domain (Figure S4C), however these
319 were not in the same location as those observed within the narrower periplasm. Interactions of
320 HasB periplamic region (*i.e.* residues 90-256, a part of the proline-rich domain and $HasB_{CTD}$) and
321 POPE lipids were also observed in these simulations (Figure S2B). These data not only show that
322 the HasR-HasB interactions are stable in the wide periplasm, but also that the HasB proline-rich
323 domain has considerable conformational flexibility and can likely adopt a range of conformations at
324 different steps of the mechanism.

325

326 **Effect of the presence of heme and HasA on the HasR-HasB interaction**

327 The heme internalization through HasR and the ejection of HasA need the energy that is provided
328 by HasB through the HasR-HasB interaction. In a previous study, we showed that the presence of
329 heme and HasA on the extracellular side of HasR modified its interaction with HasB[14]. Here, in
330 order to get insight into this signaling process and identify the interactions that are modified, we
331 performed molecular dynamics simulations of the interaction of HasR loaded with HasA and heme
332 (holoHasA) with HasB. We performed 2 x 300 ns simulations of the holoHasR-HasB system. Given
333 the importance of the D_{100}-R_{169} salt bridge for the heme internalization *via* HasR, we analysed the
334 trajectory in which this salt bridge is most stable.

335 As in the apo-form, at the early stage of the simulation L4 and L1 of the holoHasR interact with
336 HasB. Whereas the L1-HasB interaction stays stable during the simulation, the interaction with L4
337 is lost. Instead, the loop 10 (L10) binds to HasB. This interaction involves $D_{777}R_{778}K_{779}$ of HasR L10
338 and $R_{223}E_{224}$ of HasB, and stays stable during the simulation (Figure 4 C, 4D).

339 In order to further understand the importance of L10 in this interaction, we performed molecular
340 dynamics simulations with a variant of holoHasR in which L10 residues (R_{774}AFDRKLD) were
341 replaced by ATSA. Interestingly in this mutant, the L4-HasB interaction is formed and remains
342 stable. Although in this mutant complex, the residues of HasB interacting with L4 are different from
343 those in the HasR-HasB simulations presented above (R_{178}, R_{181}, R_{188} *versus* $K_{230}R_{231}$), the
344 orientation of HasB with the respect of the β barrel is similar, suggesting a preferred orientation

345 (Figure S5). During these simulations, the salt bridge between the TonB-box and HasB is stable,
346 and the HasB-HasR barrel and $HasR_{SD}$-barrel distances are comparable to that observed in other
347 complexes in this study.
348
349 **Experimental validation of the role of HasR loops in the HasR-HasB interaction**
350 In previous work, we studied a HasR mutant in which the TonB-box was deleted ($HasR_{\Delta TBB}$).
351 Although $HasR_{\Delta TBB}$ was not functional *in vivo*, it was still able to bind to $HasB_{CTD}$ *in vitro,* but with
352 significantly less affinity (16) and lower ΔH (Figure 5). We concluded that besides the TonB-box,
353 other regions of HasR are recognized by HasB. In the present study, the simulations revealed the
354 importance of HasR periplasmic loops L1, L4 and L10 in the HasR-HasB interaction. Here we
355 measured the thermodynamic parameters of the interaction between $HasB_{CTD}$ and variants of HasR
356 in which the sequence of L1 (P_{232}GKE), L4 (P_{392}EDVDWLD) or L10 (R_{774}AFDRKLD) were
357 substituted by ATSA. These variants lacked the whole N-terminal region containing $HasR_{SD}$ and
358 the TonB-box ($HasR_{\Delta Nter}$), to evaluate only the contribution of periplasmic loops in the interaction.
359 The HasR mutants $HasR_{\Delta Nter\text{-}L1}$, $HasR_{\Delta Nter\text{-}L4}$, $HasR_{\Delta Nter\text{-}L10}$ were prepared and purified by using the
360 same protocol as for the wild type, indicating that they were well folded and inserted into the OM.
361 The effect of the L4 mutation is drastic, as only a small endothermic signal that could correspond
362 to a heat of dilution was observed in the ITC experiment with $HasR_{\Delta Nter\text{-}L4}$ and $HasB_{CTD}$ (Figure 5
363 top). In the simulations, HasR L4 forms polar interactions and salt bridges with $K_{230}R_{231}$ of HasB.
364 Similarly, the ITC titration of $HasB_{CTDK230AR231A}$ and $HasR_{\Delta Nter}$ show an endothermic signal (Figure
365 S6). The enthalpic signal reflects the contribution of polar interactions. The loss of the enthalpic
366 signal observed with these mutants compared to the ΔH value (-7.3 $kcal.mol^{-1}$) measured for the
367 $HasR_{\Delta TBB}$-$HasB_{CTD}$ interaction is compatible with at least two salt bridges that could correspond to
368 the contribution of the HasR L4-HasB $K_{230}R_{231}$ interaction.
369 $HasR_{\Delta Nter\text{-}L10}$ still interacts with $HasB_{CTD}$, although with less affinity (3.7 times) and with a loss of
370 polar interactions compared to $HasR_{\Delta TBB}$ (ΔH -2.9 *versus* -7.3 $kcal.mol^{-1}$) (Figure 5). In the
371 simulations, HasR L10 residues form salt bridge and polar interactions with HasB $R_{223}E_{224}$.
372 Unfortunately, the $HasB_{CTD}$ variant in which these charged residues are replaced by neutral ones,
373 oligomerises and is not stable as monomer. Therefore, we could not study the interaction of this
374 mutant with HasR *in vitro* by ITC.
375 $HasR_{\Delta Nter\text{-}L1}$ interacts with $HasB_{CTD}$ with comparable thermodynamic parameters as $HasR_{\Delta TBB}$
376 showing that the substitution in L1 has no effect on the binding and on the contribution of polar

interactions. This is consistent with the simulations showing that this loop interacts with $HasB_{CTD}$ by mostly hydrophobic contacts.

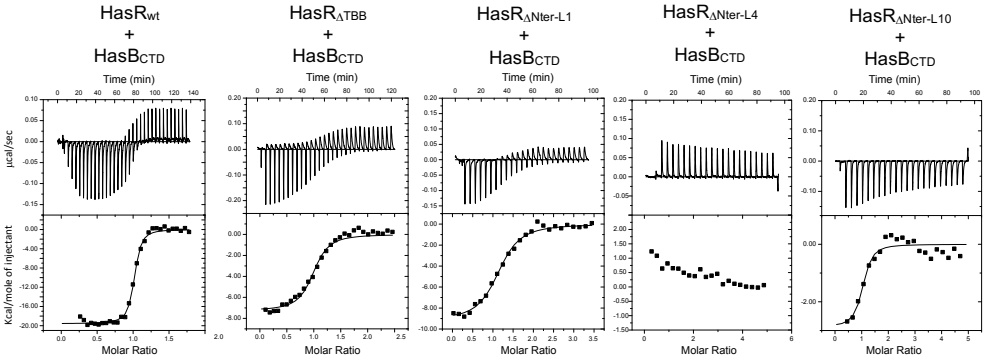

Binding partners	N	Ka (M^{-1})	DH ($kcal.mol^{-1}$)
$HasR_{wt}$ + $HasB_{CTD}$	1.03	7.5 (± 0.2) x 10^7	-19.1 ± 0.24
$HasR_{\Delta TBB}$ + $HasB_{CTD}$	0.98	3.9 (± 0.8) x 10^6	-7.3 ± 0.18
$HasR_{\Delta Nter\text{-}L1}$ + $HasB_{CTD}$	1.1	3.03 (± 0.4) x 10^6	-9.2 ± 0.19
$HasR_{\Delta Nter\text{-}L4}$ + $HasB_{CTD}$	ND	ND	ND
$HasR_{\Delta Nter\text{-}L10}$ + $HasB_{CTD}$	0.98	1.45 (± 1.0) x 10^7	-2.9 ± 0.35

***Figure 5. ITC analysis of the interaction of $HasB_{CTD}$ with different variants of HasR**. Top: Representative experiments are shown. In each case, the heat signal is shown together with the binding isotherm derived from the signal. Bottom: Stoichiometries (N), affinity constants (Ka) and ΔH of binding at 25°C are shown. ND: not determined.*

To assess the importance of HasR L4 and L10 in the mechanism of heme entry, we monitored the growth of *E. coli* strain *K12* C600Δ*hemA*Δ*tonB* that needed an external source of heme (here 0.4µM heme-BSA) and expressed the complete has locus (*hasISRADEB*) with either *hasR* wild type or mutated in L4 ($HasR_{L4}$) or in L10 ($HasR_{L10}$). A mutant in L3 ($HasR_{L3}$) was used as a control. The complete *has* allows the expression of all Has proteins required for the secretion of HasA (*hasA, hasD, hasE*), heme internalisation (*hasR, hasB*) and the transcription regulation of the system (*hasI, hasS*). In this *E. coli* strain *tonBexbBexbD* were removed and *exbBexbD* from *S. marcescens* was added (HasB partners in the IM) in order to have a fully functional HasB.

The growth curves with the expression of the HasR wild type, $HasR_{L3}$, $HasR_{L4}$ or $HasR_{L10}$ are shown in Figure 6. The mutation on HasR L4 and L10 significantly affect the bacterial growth curve (Figure 6A). $HasR_{L3}$ is used as a control. The expression level of all variants is comparable to that of the wild type, indicating that the mutations do not modify the overall folding of the protein (Figure 6A). The lag phase is significantly longer with $HasR_{L4}$ (9.5h) and $HasR_{L10}$ (25h) versus 5.5h for the wild type and $HasR_{L3}$. In addition, with the two variants $HasR_{L4}$ and $HasR_{L10}$, the OD600 do not reach

399 the maximum obtained with the wild type HasR. The most important effect was observed with
400 $HasR_{L10}$ where only an OD600 at 0.1 is reached after 40h of growth, compared to the wild type with
401 an OD600 at 0.57 after 25h. These observations are consistent with the key role of L4 and L10 in
402 the interaction with HasB revealed by our simulations and observed in ITC experiments.
403 In the simulations, L4 forms stable polar interactions and salt bridges with $K_{230}R_{231}$ of HasB, and
404 L10 with $R_{223}E_{224}$. We substituted these charged residues to alanine and tested the activity of the
405 mutants $HasB_{K230AR231A}$ and $HasB_{R223AE224A}$ *in vivo* (Figure 6A). These mutants give comparable
406 phenotype than the $HasR_{L4}$ and $HasR_{L10}$ variants, although the level of $HasB_{R223AE224A}$ expression
407 and/or stability is lower than that of the wild type (Figure 6B).
408 Together the *in vivo* results confirm the key role of HasR L4 and L10 in the interaction with $HasB_{CTD}$
409 and in the HasR function.
410

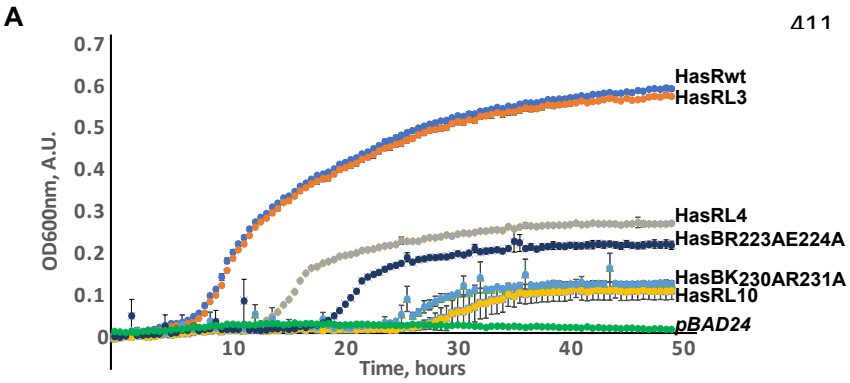

418
419 B
420
421
422
423
424

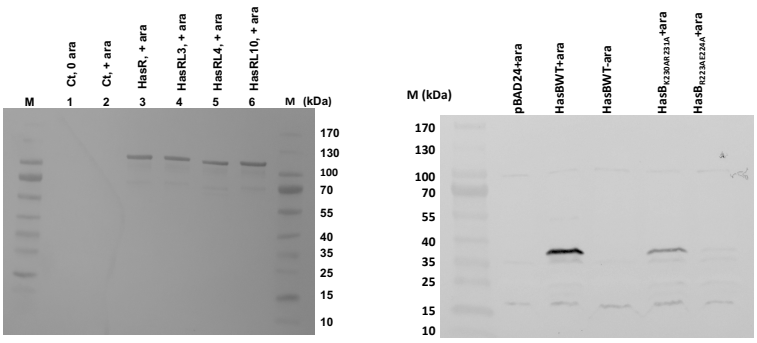

425 ***Figure 6. Phenotypic analysis of HasR periplasmic loops substitution in vivo. A:*** *Growth*
426 *curves of E. coli C600 ΔhemAΔtonBΔexbBD harbouring pBAD24 vector (negative control) or its*
427 *derivatives encoding* $exbBD_{sm}$ *and the wild type has locus (HasR wt), HasR derivatives with HasR*
428 *L3, L4 or L10 substitution or HasB derivatives are presented and labelled.* ***B:*** *Top, Immunodetection*
429 *with polyclonal anti-HasR rabbit antibody in C600ΔhemA transformed with either pBAD24 (negative*
430 *control, line 1 and 2), pFR2 (*$HasR_{wt}$*, line 3), pFR2:* $HasR_{L3}$*, pFR2:* $HasR_{L4}$ *or pFR2:* $HasR_{L10}$*. Cells*
431 *were inoculated at 0.05* OD_{600nm} *in LB medium containing δ-aminolevulinic acid (25 µg/ml) at 37°C*
432 *for 3 hours. An equivalent of 0.1 OD600nm was loaded on each lane. Arabinose (Ara) concentration*

433 *was 40µg/ml. Molecular mass of standard weight markers is indicated on the right. Bottom:*
434 *Expression level of HasB, HasB$_{K230AR231A}$, HasB$_{R223AE224A}$ measured by immunodetection with*
435 *polyclonal anti-HasB rabbit antibody in the E. coli K12 strain JP313 (ΔaraBAD) was used and*
436 *transformed with a plasmid expressing ExbBD from S. marcescens and another plasmid*
437 *expressing HasB or its mutants or a control plasmid (pBAD24). Induction was with 40µg/ml*
438 *arabinose for two hours at 37°C. The equivalent of 0.15 OD$_{600nm}$ was loaded on each lane. After*
439 *transfer on a nitrocellulose membrane and incubation with the primary antibody (1/5000 dilution),*
440 *the immunoblots were revealed with goat anti-rabbit IgG coupled to alkaline phosphatase.*

441

442 **Discussion**

443 Our study reveals the key role of specific periplasmic loops of a TBDT in its interaction with a TonB
444 protein and in its function. Moreover, the simulations show that the involved loops and the sequence
445 of the events are different depending on the presence of the extracellular substrates, heme and
446 HasA. This implies that the conformational and dynamics changes associated to substrate binding
447 on the extracellular side of HasR are transmitted through the barrel and plug to the periplasmic side
448 of HasR and the region of interaction with HasB.

449 In the absence of extracellular substrates, the interaction of HasR L1 and HasB occurs very early,
450 mainly *via* hydrophobic contacts. Once these contacts are formed, the HasR linker and HasB move
451 with respect to each other (mostly through HasB rotation) such that HasB contacts L4 (Movie S1).
452 The HasR-HasB interaction is then stabilized through several salt bridges between L4 and HasB
453 $K_{230}R_{231}$ residues (Figure 4A). When the charged residues involved in this interaction were replaced
454 by neutral residues, either in HasB (HasB$_{K230AR231A}$) or in HasR (HasR$_{L4}$) the bacterial growth is
455 significantly affected (Figure 6), suggesting the key role of the L4-HasB interaction in heme import
456 and/or signalling through HasR. The ITC experiments showed also that L4 is required for HasR-
457 HasB complex formation and stability (Figure 5). The HasR L4-HasB interaction seems to stabilise
458 the salt bridge between the HasR TonB box and HasB, since in the simulations with HasR$_{L4}$, this
459 salt bridge is not maintained. As shown previously, this salt bridge is required for HasR function *in*
460 *vivo* (16).

461 When the extracellular substrates are present on HasR (holoHasR), although L4 and L1 form
462 interactions with HasB quickly, the interactions with L4 are disrupted while those with L1 are
463 maintained. Instead, L10 residues form polar and ionic interactions with HasB (Figure 4C). We
464 validated the key role of L10 and of its charged residues in the interaction with HasB *in vitro* and
465 with functional *in vivo* assays (Figure 5 & 6). Interestingly in the simulation where the charged
466 residues of L10 are substituted by neutral ones (holoHasR$_{L10}$-HasB), instead of L10-HasB, the L4-
467 HasB interaction is formed (Figure S5). This is consistent with the *in vivo* data showing that the
468 substitution in L10 or L4 does not completely abolish the heme acquisition and suggests that L4
469 and L10 can be involved in different steps of the heme acquisition and might be partially

470 interchangeable. In our simulations, the L10-HasB interaction occurs only when HasR is in its holo-
471 form. This interaction could be crucial for the step of heme internalisation and the ejection of HasA,
472 two steps for which energy is required.
473 Structural data showed that the TonB-TBDT interaction involves a salt bridge between the TonB-
474 box of the transporter and TonB, stabilizing an inter-protein β-sheet (4),(6),(7),(15). Both salt bridge
475 and the inter-protein β-sheet were shown important for the energy transfer from the TonB protein
476 to the transporter (20),(21). In all the simulations presented here, the salt bridge between HasR and
477 HasB and the inter-protein β-sheet are formed, although sometimes they are observed to disrupt
478 and reform. They are more stabilised once HasB contact HasR periplasmic loops (Figure 3).
479 Simulations of HasR in an OM model containing lipopolysaccharide (LPS) at the Ra-LPS level (*i.e.*
480 without the O-antigen group) showed very little motion of the protein in 500 ns (Figure S7). This is
481 not surprising given the slow-moving nature of LPS. While we and others have reported that the
482 conformational behaviour of TBDTs can be altered by the presence of LPS (22, 23) , the large size
483 of the systems we have studied here, would require simulations considerably beyond the scope of
484 the present study to explore any impact of LPS.
485 If we compare the HasB-HasR interaction network with the sequence and the structure of other
486 available TBDT-TonB complexes (PDB entries 2GSK, 2GRX and 6I97), the residues of HasR L1,
487 L4 - notably the charged residues of L4- are well conserved in FoxA, BtuB and FhuA, although the
488 loops are slightly shorter in these proteins compared to those of HasR. L10 is less conserved
489 (Figure S8). The HasB residues that contact L1, L4 and L10 in our simulations are also well
490 conserved and exposed at the surface of *E. coli* and *P. aeruginosa* TonB (Figure 7). However, no
491 simultaneous interactions between TBDT L1 and L4/L10 with TonB are observed in these complex
492 structures. This may be a result of only the globular C-terminal part of TonB being used in these
493 studies. In our full-length model of HasB inserted into the IM, the dynamics of its periplasmic domain
494 attached to the IM allows a more thorough exploration of the exposed surface of HasR and the
495 simultaneous interaction of HasB with L1 and L4 or L10. Therefore, we hypothesise that the HasR-
496 HasB interacting mode revealed in this study can occur in other TBDT-TonB interactions.
497 The energizing mechanism used by Gram-negative bacteria to internalize scarce and essential
498 nutrients is still not well deciphered. Understanding it will help the future development of new
499 antibacterial strategies. It is assumed that energized TonB applies a mechanical force to remodel
500 the TBDT plug and open a channel through the barrel, allowing substrate entry. How TonB applies
501 this force is not yet understood. EPR (24) and AFM (21) data, as well as steered molecular
502 dynamics (20) support a pulling movement of TonB, while a recent structural study suggests a
503 rotational model based on structural homology to the Mot flagellar system (9). During our
504 simulations, we observed the rotation of HasB with respect to HasR, while the $HasB_{CTD}$-HasR barrel
505 distance remains stable (4-5 nm in all the simulations). These observations may suggest a

rotational model, rather than a pulling model for which a variation of the $HasB_{CTD}$-HasR barrel distance would have been expected. However, the simulations are performed in the absence of ExbB and ExbD, the partners of HasB in the IM, and without the input of energy. Further studies with ExbB and ExbD will thus be required to fully understand the mechanism of energy transfer between the two bacterial membranes.

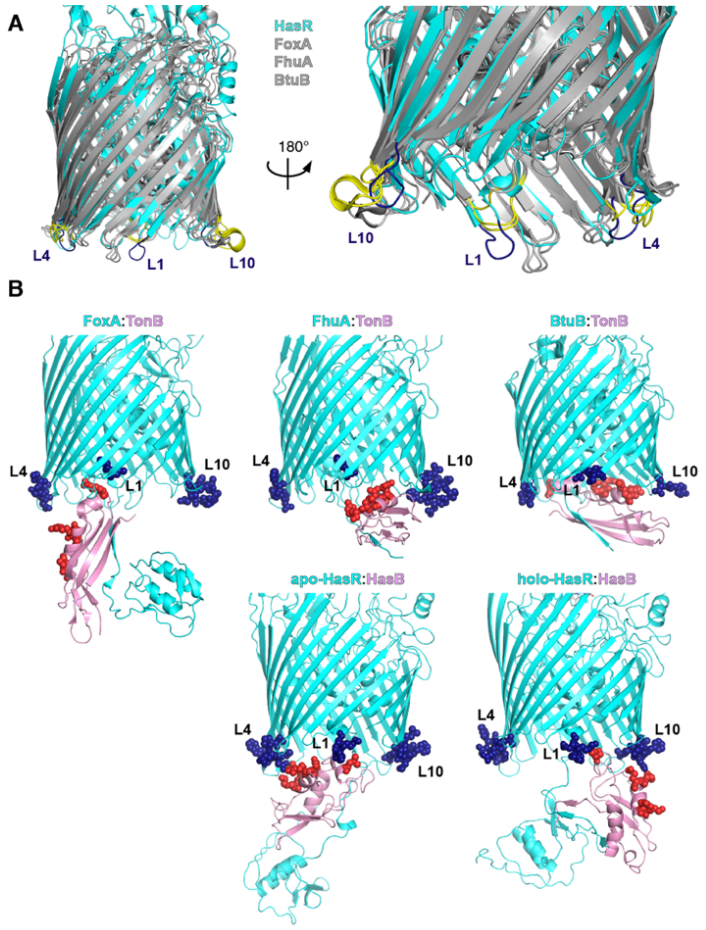

Figure 7. Periplasmic loops in TBDT in complex with TonB. (A) *Superposition of TBDT structures HasR (cyan), FoxA, FhuA and BtuB (grey). Loops L1, L4 and L10 of HasR are coloured in dark blue while the corresponding residues in FoxA, FhuA and BtuB are coloured in yellow.* ***(B)*** *Transporters (cyan) in complex with the C-terminal domain of TonB/HasB (pink) are depicted in cartoon. The residues of loops L1, L4 and L10 are shown in blue spheres. Residues of TonB equivalent to the ones from HasB interacting with HasR in MD simulations (i.e. HasB L_{189}, R_{223}, E_{224}, K_{230} and R_{231}) are shown as red spheres.*

539 **Materials and Methods**

540

541 **Positioning the protein complex in the membranes**

542 The CHARMM-GUI web-server (25)·(26) was used to assemble the lipid bilayers, both as squares
543 with side-length 16.5 nm. The inner membrane was made up of two leaflets of 1-pamitoyl-2-oleoyl-
544 sn-glycero-3-phosphoethanolamine (POPE). The outer membrane similarly had a lower leaflet of
545 POPE but an upper leaflet of 1,2-dilauroyl-sn-glycero-3-phosphocholine (DLPC) as the tail lengths
546 of DLPC are similar to those of lipopolysaccharide (which is found in the outer leaflet *in vivo*, but
547 requires long simulations to achieve convergence and thus was not used here as our interest was
548 in the protein complex rather than specific details of protein-outer membrane interactions)(27). The
549 two membranes were subjected to a 5000-step energy minimisation using the steepest descents
550 algorithm.

551 To align the HasR barrel in the outer membrane, co-ordinates were taken from the MemProtMD
552 database (28) and used for alignment to ensure the lipid headgroups were in the correct position
553 relative to the protein. The location of the HasB helix in the inner membrane was estimated by
554 using the location of the tryptophan residues, given there was no structural information available
555 for this section (29).

556 Simulations involving HasR and HasB were set up as follows; once the proteins had been inserted
557 into the membranes, any overlapping lipids were removed prior to energy minimisation. The
558 CHARMM-GUI webserver was used to generate the necessary topology and parameter files for all
559 models and structures reported in this study.

560

561 **Molecular Dynamics Simulations**

562 The systems were solvated with the TIP3P water model. K^+ and Cl^- ions were added to achieve an
563 overall concentration of 150 mM in charge neutral systems. The systems were then subjected to a
564 short energy minimisation of 5000 steps, again by using the steepest descent algorithm, to remove
565 any steric clashes, followed by an equilibration protocol as shown in Table S1. This protocol, with
566 slow relaxing of the restraints on the protein was necessary to allow the lipids to equilibrate around
567 the proteins.

568 All simulations were carried out with the GROMACS 2019.6 (30) version (www.gromacs.org) and
569 CHARMM36 (31) forcefield. The long-range electrostatic interactions were treated by using the
570 Particle Mesh Ewald (PME)(32) method, whereas the nonbonded interactions and the short-range
571 electrostatics were cut off at 1.2 nm, applied by using the potential shift Verlet cut off scheme. The
572 temperature was maintained at 303.15 K by using the Nosé-Hoover thermostat (33)(34) with a 5 ps
573 coupling constant. To maintain a constant pressure at 1 atm, the Parrinello-Rahman barostat (35)
574 was applied in a semi-isotropic fashion, again with a coupling constant of 5ps. The LINCS (36)

575 algorithm was applied to all atoms to allow the time step of 2 fs. Table 1 shows the summary of
576 production runs, all of which were run in the NPT ensemble.
577
578
579 Table 1: Summary of the Equilibrium MD Simulation Systems

System	Temperature (K)	Simulation Length (ns)
HasR + HasB	303.15	300 (x2)
*Int-HasR + HasB	303.15	300 (x4)
holoHasR +HasB	303.15	300 (x2)
$HasR_{L4}$+ HasB	303.15	150 (x2)
$HasR_{L10}$+ HasB	303.15	150 (x2)
**Int-HasR + HasB in the wide periplasm	303.15	50 (x2)
***HasR + LPS	303.15	500 (x2)

580
581 *The int HasR_HasB simulations were initiated from a structure extracted after 100 ns from one of
582 the HasR + HasB simulations after the contact with L1 and L4 had already been established.
583 **The Int-HasR + HasB in the wide periplasm simulations were initiated from the same structure as
584 the int HasR_HasB simulations, but the inner membrane with HasB helix was translated to be lower
585 ~ 8 nm. The proline-rich domain from residues 37 to 140 was remodelled by using Modeller
586 software. To allow the linker region to improve its structure, the entire protein structure, except the
587 modelled linker region, was subjected to position restraints of 1000 kJ mol^{-1}. nm^{-2} for 50 ns using
588 gromos96 54a7 force field (37). The equilibrated protein model was then placed in the double
589 membrane model, followed by a short equilibration with a position restraint of 50 kJ mol^{-1} nm^{-2} on
590 the backbone for 10 ns by using CHARMM36 forcefield.
591 ***The HasR + LPS simulations were built by embedding the HasR barrel and plug domain (PDB
592 entry 3CSL) in the outer membrane with the predefined LPS model of *E. coli* in CHARMM-GUI.
593 The lower leaflet of the outer membrane contains POPE, 1-palmitoyl 2-cis-vaccenic
594 phosphatidylglycerol (POPG) and tetraoleoyl cardiolipin (TOCL2) in the ratio 18:1:1 (38)·(39), while
595 the upper leaflet of the outer membrane contains a predefined Ra-LPS model of *E. coli* available
596 in CHARMM-GUI (26, 27). The HasR with the Ra-LPS model was then subjected to the equilibration
597 steps shown in the Table S1.
598

599 **Isothermal Titration Calorimetry (ITC)**

600 ITC experiments were performed at 25°C by using a MicroCal VP titration calorimeter (MicroCal-
601 GE Healthcare) under the same conditions as described previously (16). The buffer was 20 mM
602 sodium phosphate, pH 7, 0.08% Zwittergent 3–14 for all titrations. All protein samples were dialyzed
603 in this buffer before the experiments. Consecutive aliquots of 5-10 µL of $HasB_{CTD}$ at 80-120 µM
604 were added into the ITC cell containing HasR wild type or mutant proteins at 4-15 µM. The heat of
605 dilution of protein injections was determined either by injecting the ligand into the buffer alone or
606 by injecting the ligand into the cell after the saturation of the protein binding site. The value obtained
607 was subtracted from the heat of reaction to give the effective heat of binding. The resulting titration
608 data were analysed by using the Microcal-ORIGIN software package. The molar binding
609 stoichiometry (N), association constant (Ka; Kd =1/Ka) and enthalpy changes (ΔH) of binding were
610 determined by fitting the binding isotherm to a model with one set of sites. All experiments were
611 done in duplicate.

612

613 **Bacterial growth test**

614 Growth tests in liquid medium were performed with *E. coli* C600 Δ*hemA*Δ*tonB*Δ*exbBD* strain
615 harbouring vector pAMhasISRADEB encoding the whole has locus (*hasISRADEB)* and including
616 either the wild type *hasr* or a mutant. The expression of this vector is under Fur regulation, induced
617 in iron deficiency conditions. An additional *vector* pBAD24exbBDsm encoding *E*xbB and ExbD from
618 *S. marcescens*, under the control of the P_{araBAD} promoter was also present. A few colonies of this
619 strain were first inoculated in 4ml of LB medium at 37°C with 100µM dipyridyl (an iron chelator),
620 4µg/ml arabinose and the corresponding antibiotics. Once the culture reached an OD_{600nm} between
621 1.2-1.5, it was diluted and inoculated in 48 well Greiner plates, in the same medium to which was
622 added 0.4µM He-BSA, as a heme source. The initial OD_{600nm} of the cultures was 0.001. Each well
623 contained 300µl of growth medium. Duplicates of each strain were made, and the plate was
624 incubated at 37°C with vigorous shaking (500rpm) in a Clariostar Plus Microplate reader. OD_{600nm}
625 was recorded every 30 minutes for 70 hours. All experiments were performed in triplicate. In the
626 expression test of HasR and his mutants, δ-aminolevulinic acid, a heme synthesis precursor was
627 added to the culture at 25µg/ml.

628

629

630 **Acknowledgments**

631 This work was funded by the French Agence Nationale de la Recherche ANR
632 HemeStockExchange, the Fondation pour la Recherche Médicale (Equipe FRM
633 2017M.DEQ20170839114). K.S is funded by the Development and Promotion of Science and
634 Technology Talents Project (DPST), Thailand. SK is funded by the EPSRC grant number

EP/R029407. The PD and AP lab is supported by LABEX Dynamo (LABEX DYNAMO ANR-11-LABEX-0011-01). We thank Christophe Thomas from the platform of production and purification of recombinant proteins at the Institut Pasteur for bacterial cell production in fermentor, the platform of molecular biophysics at the Institut Pasteur for providing access to the microcalorimeter and Loïc Hellio for HasB sample preparation. We thank Riccardo Pellarin for helpful discussions. The authors acknowledge the use of the IRIDIS High Performance Computing Facility, and associated IT support services at the University of Southampton.

References

1. N. Noinaj, M. Guillier, T. J. Barnard, S. K. Buchanan, TonB-dependent transporters: regulation, structure, and function. *Annu Rev Microbiol* **64**, 43–60 (2010).
2. V. Braun, Energy-coupled transport and signal transduction through the gram-negative outer membrane via TonB-ExbB-ExbD-dependent receptor proteins. *FEMS Microbiol Rev* **16**, 295–307 (1995).
3. A. C. Ratliff, S. K. Buchanan, H. Celia, Ton motor complexes. *Curr Opin Struct Biol* **67**, 95–100 (2021).
4. R. Sean Peacock, A. M. Weljie, S. Peter Howard, F. D. Price, H. J. Vogel, The solution structure of the C-terminal domain of TonB and interaction studies with TonB box peptides. *J Mol Biol* **345**, 1185–1197 (2005).
5. J. S. Oeemig, O. H. S. Ollila, H. Iwaï, NMR structure of the C-terminal domain of TonB protein from Pseudomonas aeruginosa. *PeerJ* **6**, e5412 (2018).
6. P. D. Pawelek, *et al.*, Structure of TonB in complex with FhuA, E. coli outer membrane receptor. *Science* **312**, 1399–1402 (2006).
7. D. D. Shultis, M. D. Purdy, C. N. Banchs, M. C. Wiener, Outer membrane active transport: structure of the BtuB:TonB complex. *Science* **312**, 1396–1399 (2006).
8. I. Josts, K. Veith, H. Tidow, Ternary structure of the outer membrane transporter FoxA with resolved signalling domain provides insights into TonB-mediated siderophore uptake. *Elife* **8** (2019).
9. J. C. Deme, *et al.*, Structures of the stator complex that drives rotation of the bacterial flagellum. *Nat Microbiol* **5**, 1553–1564 (2020).
10. C. Wandersman, P. Delepelaire, Haemophore functions revisited. *Mol Microbiol* **85**, 618–631 (2012).
11. W. Huang, A. Wilks, Extracellular Heme Uptake and the Challenge of Bacterial Cell Membranes. *Annu Rev Biochem* **86**, 799–823 (2017).

670 12. M.-S. Rossi, A. Paquelin, J. M. Ghigo, C. Wandersman, Haemophore-mediated signal
671 transduction across the bacterial cell envelope in Serratia marcescens: the inducer and the
672 transported substrate are different molecules. *Mol Microbiol* **48**, 1467–1480 (2003).
673 13. H. Wojtowicz, *et al.*, Structural basis of the signalling through a bacterial membrane receptor
674 HasR deciphered by an integrative approach. *Biochem J* **473**, 2239–2248 (2016).
675 14. S. Krieg, *et al.*, Heme uptake across the outer membrane as revealed by crystal structures of
676 the receptor-hemophore complex. *Proc Natl Acad Sci U S A* **106**, 1045–1050 (2009).
677 15. G. C. de Amorim, *et al.*, The structure of HasB reveals a new class of TonB protein fold. *PLoS*
678 *One* **8**, e58964 (2013).
679 16. J. Lefèvre, P. Delepelaire, M. Delepierre, N. Izadi-Pruneyre, Modulation by substrates of the
680 interaction between the HasR outer membrane receptor and its specific TonB-like protein,
681 HasB. *J Mol Biol* **378**, 840–851 (2008).
682 17. K. A. Sochacki, I. A. Shkel, M. T. Record, J. C. Weisshaar, Protein Diffusion in the Periplasm
683 of E. coli under Osmotic Stress. *Biophys J* **100**, 22–31 (2011).
684 18. V. R. F. Matias, A. Al-Amoudi, J. Dubochet, T. J. Beveridge, Cryo-Transmission Electron
685 Microscopy of Frozen-Hydrated Sections of Escherichia coli and Pseudomonas aeruginosa.
686 *Journal of Bacteriology* **185**, 6112–6118 (2003).
687 19. S. Murakami, R. Nakashima, E. Yamashita, A. Yamaguchi, Crystal structure of bacterial
688 multidrug efflux transporter AcrB. *Nature* **419**, 587–593 (2002).
689 20. J. Gumbart, M. C. Wiener, E. Tajkhorshid, Mechanics of force propagation in TonB-
690 dependent outer membrane transport. *Biophys J* **93**, 496–504 (2007).
691 21. S. J. Hickman, R. E. M. Cooper, L. Bellucci, E. Paci, D. J. Brockwell, Gating of TonB-
692 dependent transporters by substrate-specific forced remodelling. *Nat Commun* **8**, 14804
693 (2017).
694 22. C. Balusek, J. C. Gumbart, Role of the Native Outer-Membrane Environment on the
695 Transporter BtuB. *Biophys J* **111**, 1409–1417 (2016).
696 23. T. J. Piggot, D. A. Holdbrook, S. Khalid, Conformational dynamics and membrane interactions
697 of the E. coli outer membrane protein FecA: a molecular dynamics simulation study. *Biochim*
698 *Biophys Acta* **1828**, 284–293 (2013).
699 24. J. L. Sarver, M. Zhang, L. Liu, D. Nyenhuis, D. S. Cafiso, A Dynamic Protein-Protein Coupling
700 between the TonB-Dependent Transporter FhuA and TonB. *Biochemistry* **57**, 1045–1053
701 (2018).
702 25. B. R. Brooks, *et al.*, CHARMM: The biomolecular simulation program. *J. Comput. Chem.* **30**,
703 1545–1614 (2009).
704 26. S. Jo, T. Kim, V. G. Iyer, W. Im, CHARMM-GUI: a web-based graphical user interface for
705 CHARMM. *J Comput Chem* **29**, 1859–1865 (2008).

27. J. Lee, *et al.*, CHARMM-GUI Membrane Builder for Complex Biological Membrane Simulations with Glycolipids and Lipoglycans. *J Chem Theory Comput* **15**, 775–786 (2019).
28. J. Maupetit, P. Tuffery, P. Derreumaux, A coarse-grained protein force field for folding and structure prediction. *Proteins* **69**, 394–408 (2007).
29. A. J. Situ, *et al.*, Membrane Anchoring of α-Helical Proteins: Role of Tryptophan. *J Phys Chem B* **122**, 1185–1194 (2018).
30. D. Van Der Spoel, *et al.*, GROMACS: fast, flexible, and free. *J Comput Chem* **26**, 1701–1718 (2005).
31. J. Huang, A. D. MacKerell, CHARMM36 all-atom additive protein force field: validation based on comparison to NMR data. *J Comput Chem* **34**, 2135–2145 (2013).
32. E. Fadrná, K. Hladečková, J. Koča, Long-range Electrostatic Interactions in Molecular Dynamics: An Endothelin-1 Case Study. *Journal of Biomolecular Structure and Dynamics* **23**, 151–162 (2005).
33. null Hoover, Canonical dynamics: Equilibrium phase-space distributions. *Phys Rev A Gen Phys* **31**, 1695–1697 (1985).
34. S. Nosé, A unified formulation of the constant temperature molecular dynamics methods. *The Journal of Chemical Physics* **81**, 511–519 (1984).
35. M. Parrinello, A. Rahman, Polymorphic transitions in single crystals: A new molecular dynamics method. *Journal of Applied Physics* **52**, 7182–7190 (1981).
36. Hess, (Berk), Bekker, (Henk), Berendsen, (Herman J. C.), Fraaije, (Johannes G. E. M.), LINCS: A linear constraint solver for molecular simulations.
37. N. Schmid, *et al.*, Definition and testing of the GROMOS force-field versions 54A7 and 54B7. *Eur Biophys J* **40**, 843–856 (2011).
38. D. Spittell, L. K. Vongroven, M. T. Subbiah, Concentration changes of bile acids in sequential segments of pigeon intestine and their relation to bile acid absorption. *Biochim Biophys Acta* **441**, 32–37 (1976).
39. K. Yokota, R. Kanamoto, M. Kito, Composition of cardiolipin molecular species in Escherichia coli. *J Bacteriol* **141**, 1047–1051 (1980).